The T-type Ca2+ Channel Cav3.2 Regulates Differentiation of Neural Progenitor Cells during Cortical Development via Caspase-3

Rebellato, Paola; Kaczynska, Dagmara; Kanatani, Shigeaki; Rayyes, Ibrahim Al; Zhang, Songbai; Villaescusa, Carlos; Falk, Anna; Arenas, Ernest; Hermanson, Ola; Louhivuori, Lauri; Uhlén, Per

Published in:
Neuroscience

DOI:
10.1016/j.neuroscience.2019.01.015

2019

Document Version:
Publisher's PDF, also known as Version of record

NEUROSCIENCE
RESEARCH ARTICLE
P. Rebellato et al. / Neuroscience 402 (2019) 78–89

The T-type Ca^{2+} Channel $Ca_v3.2$ Regulates Differentiation of Neural Progenitor Cells during Cortical Development via Caspase-3

Paola Rebellato,[a†] Dagmara Kaczynska,[a†] Shigeaki Kanatani,[a] Ibrahim Al Rayyes,[a] Songbai Zhang,[a] Carlos Villaescusa,[a] Anna Falk,[b] Ernest Arenas,[a] Ola Hermanson,[b] Lauri Louhivuori[a*] and Per Uhlén[a*]

[a] *Department of Medical Biochemistry and Biophysics, Karolinska Institutet, SE-171 77 Stockholm, Sweden*

[b] *Department of Neuroscience, Karolinska Institutet, SE-171 77 Stockholm, Sweden*

Abstract—Here we report that the low-voltage-dependent T-type calcium (Ca^{2+}) channel $Ca_v3.2$, encoded by the *CACNA1H* gene, regulates neuronal differentiation during early embryonic brain development through activating caspase-3. At the onset of neuronal differentiation, neural progenitor cells exhibited spontaneous Ca^{2+} activity. This activity strongly correlated with the upregulation of *CACNA1H* mRNA. Cells exhibiting robust spontaneous Ca^{2+} signaling had increased caspase-3 activity unrelated to apoptosis. Inhibition of $Ca_v3.2$ by drugs or viral *CACNA1H* knock down resulted in decreased caspase-3 activity followed by suppressed neurogenesis. In contrast, when *CACNA1H* was overexpressed, increased neurogenesis was detected. Cortical slices from *Cacna1h* knockout mice showed decreased spontaneous Ca^{2+} activity, a significantly lower protein level of cleaved caspase-3, and microanatomical abnormalities in the subventricular/ventricular and cortical plate zones when compared to their respective embryonic controls. In summary, we demonstrate a novel relationship between $Ca_v3.2$ and caspase-3 signaling that affects neurogenesis in the developing brain.

Key words: spontaneous Ca^{2+} activity, *Cacna1h*, neural differentiation, caspase-3, T-type calcium channels.

INTRODUCTION

At the onset of corticogenesis, radial glial cells, which are the founding cortical progenitors, increase their pool through an extend proliferation in the ventricular zone (VZ) of the cortex. As corticogenesis proceeds, radial glial cells give rise to intermediate progenitor cells that invade the subventricular zone (SVZ) (Kriegstein and Gotz, 2003; Uhlen et al., 2015). Neural progenitor cells (NPCs) go through a temporally controlled migration toward the cortical plate (CP). Here, progenitors differentiate into neuronal and glial cells and create proper connections, following a specific spatial and temporal pattern (Weissman et al., 2004). These complex events during embryonic development are strictly regulated by multiple biological mechanisms. Spontaneous fluctuations of calcium ions (Ca^{2+}), which begin to occur before the onset of chemical synaptic connections, have been linked to cell proliferation, cell differentiation, and neurotransmitter specification (Spitzer, 2006; Uhlen et al., 2015). Nonetheless, the regulation of spontaneous Ca^{2+} activity in the development of neural tissues is not fully understood, nor the biological processes that decode and transduce this activity into a physiological state (Giorgi et al., 2018; Smedler and Uhlen, 2014).

The change in the cytosolic Ca^{2+} concentration is orchestrated mainly by channels and pumps. Voltage-dependent T-type Ca^{2+} channels (Ca_v3 family) are characterized by three different α_1 subunits: $Ca_v3.1$, $Ca_v3.2$, and $Ca_v3.3$ (Perez-Reyes and Lory, 2006). T-type Ca^{2+} channels regulate various physiological processes, such as gene expression, cell proliferation and differentiation, and development of neuronal and cardiac diseases (Catterall, 2011; Senatore and Spafford, 2012; Uhlen and Fritz, 2010). For example, childhood absence epilepsy, idiopathic generalized epilepsy, and autism-spectrum disorders are correlated with polymorphism or mutations of the $Ca_v3.2$ gene *CACNA1H* (Chen et al., 2003a; Heron et al., 2007; Zhong et al., 2006). *Cacna1h*$^{-/-}$ mice exhibit many anomalous phenotypes in the central nervous system that affects brain functionality (Chen et al., 2012; Shin et al., 2008; Wang and Lewin, 2011). T-type Ca^{2+} channels are highly expressed during early development, even before the expression of the other voltage-dependent L-, N-, P/Q- and R-type Ca^{2+} channels (Louhivuori et al., 2013). It has been reported that T-type Ca^{2+} channels modulate stem cells proliferation and neuronal differentiation, but the mechanisms of

*Corresponding authors. Address: Department of Medical Biochemistry and Biophysics, Solnavägen 9, Karolinska Institutet, SE-171 77 Stockholm, Sweden. Fax: +46-8-341-960.
E-mail addresses: lauri.louhivuori@ki.se (L. Louhivuori), per.uhlen@ki.se (P. Uhlén).
† These authors contributed equally.

https://doi.org/10.1016/j.neuroscience.2019.01.015
0306-4522/

action remain largely unknown (Chemin et al., 2002; Lory et al., 2006; Rodriguez-Gomez et al., 2012).

The Cysteine-containing, Aspartate Specific ProteASES (caspases) are a class of enzymes that classically function as central regulators of apoptosis and have thus a fundamental role during morphogenesis and disease. In particular, caspase-3 is the final effector of both the mitochondrial (intrinsic) and the death receptor (extrinsic) apoptotic pathways, ending with the cleavage of many cellular substrates and induction of DNA fragmentation. Recent observations, however, reveal new roles for caspase-3 that are independent from cell death (Abdul-Ghani and Megeney, 2008; Fan et al., 2013; Fernando et al., 2005; Rohn et al., 2004). Mitochondria-dependent activation of caspase-3 has been shown to be necessary for long-term depression and AMPA (α-amino-3-hydroxi-5-metylisoxazol-4-propan syra) receptor internalization (Li et al., 2010). Upon excessive intracellular Ca^{2+} elevation, mitochondria release cytochrome C and activate the intrinsic caspase pathway. Influx through the plasma membrane due to voltage-dependent Ca^{2+} channels (VDCCs) has been shown to lead to mitochondrial disruption (Barone et al., 2004; Cano-Abad et al., 2001).

Cellular differentiation and apoptosis have some common physiological processes suggesting that the fate of a cell, for example differentiation versus cell death, could be determined by a fine regulation of the same effectors (Lanneau et al., 2007). It has been shown that caspase-3 regulates the programmed cell death in zones of the brain subjected to high proliferation during early neural development (Merendino et al., 1999; Mukasa et al., 1997; Pompeiano et al., 2000). Nonetheless, caspase-3 has also been suggested to have a function in neural development in the proliferative zones, independent to the induction of cell death (Yan et al., 2001). Additionally, placenta-derived multipotent cells differentiating into functional glutamatergic neurons were shown to have active (cleaved) caspase-3 without inducing apoptosis (Cheng et al., 2016). Here, we sought to examine what role, if any, spontaneous Ca^{2+} activity and caspase-3 have during early brain development and corticogenesis.

EXPERIMENTAL PROCEDURES

Cells

Neuronal differentiation of R1 mouse embryonic stem (mES) cells and fetal AF22 and AF24 human neuroepithelial stem (hNS) cells (Falk et al., 2012) were carried out as previously described (Gaspard et al., 2008; Shi et al., 2012; Ying et al., 2003). Cells were used only for a maximum of 20 passages to avoid chromosome aberrations.

Animals

We used the two mice strains C57BL/6 (n = 12 embryos from N = 12 mothers) and C57BL/6-129X1/SvJ (n = 10 embryos from N = 3 mothers) for *in vivo* experiments. C57BL/6 *Cacna1h* knockout (*Cacna1h*tm1Kcam) was purchased at The Jackson laboratory and as controls C57BL/6 wild-type mice were used (Janvier). Caspase-3 knockout mice with C57BL/6 background has been reported to have almost no abnormalities (Gross Abnormalities 4%, Microscopic Abnormalities 4%), whereas, 129X1/SVJ show a high rate of developmental brain abnormalities (Gross Abnormalities 78%, Microscopic Abnormalities 100%) (Leonard et al., 2002). Thus, for the phenotype analysis C57BL/6 *Cacna1h*tm1Kcam mice were crossed with 129X1/SVJ mice (The Jackson laboratory) to generate F1 C57BL/6-129X1/SvJ *Cacna1h*$^{+/-}$ animals. The F1 C57BL/6-129X1/SvJ *Cacna1h*$^{+/-}$ mice were crossed with each other to generate F2 C57BL/6-129X1/SvJ *Cacna1h*$^{-/-}$ embryos. All animal experiments were carried out under ethical approval by the Northern Stockholm Animal Research Committee (ethical no. N486/12, N40/15, 16056-2017).

Reagents

Reagents and concentrations, unless otherwise specified, were as follows: Mibefradil (3 μM or 30 μM; Tocris), KCl (12 mM; Sigma-Aldrich), Staurosporin (STS, 100 nm or 2 μM; Tocris), z-D(OMe)E(OMe)VD(OMe)-FMK (zDEVD, 2 μM or 20 μM; Tocris), and Procaspase Activating Compound-1 (PAC-1, 25 μM; Sigma).

Calcium imaging

Calcium imaging in cell cultures was performed by loading the cells with the Ca^{2+}-sensitive fluorochrome Fluo-3/AM (5 μM, Invitrogen) at 37 °C for 20 min in N2B27 medium. Measurement of intracellular Ca^{2+} was carried out in a Krebs-Ringer buffer containing 119.0 mM NaCl, 2.5 mM KCl, 2.5 mM $CaCl_2$, 1.3 mM $MgCl_2$, 1.0 mM NaH_2PO_4, 20.0 mM HEPES (pH 7.4), and 11.0 mM dextrose at 37 °C using a heat-controlled chamber (QE-1, Warner Instruments) with a cooled EMCCD Cascade II:512 camera (Photometrics) mounted on an upright microscope (Carl Zeiss) equipped with a 20× 1.0NA lens (Carl Zeiss). Excitation at 480 nm was assessed with a wavelength switcher (DG4, Sutter Instrument) at sampling frequency 0.5 Hz. MetaFluor (Molecular Devices) was used to control the whole equipment and to analyze the collected data.

Calcium imaging were performed on E16.5 embryonic brain slices, extracted from three C57BL/6 wild-type and three C57BL/6 *Cacna1h* knockout mothers, with one embryo from each mother used in the experiments (in total n = 6 embryos from N = 6 mothers). The brains were dissected from the embryos, embedded in 3% low-temperature melting agarose and cut into 300-μm slices using a Vibratome (Leica VT1000S). Tissues were kept all the time in freezing cold, bubbled cutting solution containing 62.5 mM NaCl, 2.5 mM KCl, 1.25 mM $NaH_2PO_4{\cdot}H_2O$, 25 mM $NaHCO_3$, 1 mM $CaCl_2{\cdot}2H_2O$, 4 mM $MgCl_2{\cdot}7H_2O$, 100 mM sucrose, and 10 mM glucose. Tissues recovered for 1 h at room temperature (RT) in bubbled artificial cerebrospinal fluid (ACSF) solution containing 125 mM NaCl, 2.5 mM KCl, 1.25 mM $NaH_2PO_4{\cdot}H_2O$, 25 mM $NaHCO_3$, 2 mM $CaCl_2{\cdot}2H_2O$, 1.5 mM $MgCl_2{\cdot}7H_2O$, and 0.5 M glucose. The brain

slices were bulk loaded with Fluo-4/AM (Invitrogen) in a custom-made loading chamber at 37 °C for 30 min as previously described (Malmersjo et al., 2013). Measurement of intracellular Ca^{2+} was carried out in ACSF at 37 °C using a heat-controlled chamber (QE-1, Warner Instruments) with a 2-photon laser scanning microscope (Zeiss LSM-510 NLO, Carl Zeiss, Gena, Germany). Excitation was assessed with a Ti: Sapphire Chameleon Ultra2 laser (Coherent) tuned to 810 nm at sampling frequency 0.5 Hz. The data analysis and statistic were performed using Fiji (ImageJ package software) (Schindelin et al., 2012) and MATLAB (The MathWorks Inc.). The overall Ca^{2+} activity was determined as a percentage of cells with 10% change in basal line activity.

Immunolabeling

Immunocytochemical staining was performed on mES and hNS cells using a standard protocol consisting in 20-min fixation in 4% paraformaldehyde (PFA). Cells were blocked with 5% normal goat serum, and incubated with primary antibodies: Pax6 (1:500, mouse, kind gift from Dr. Atsushi Kawakami), Nestin (1:1000, mouse, Chemicon), TuJ1 (1:200, mouse, Chemicon or Promega), and cleaved Caspase-3 (1:500, Abcam) at 4 °C overnight and then with Alexa fluorescent secondary antibodies (1:1000; Molecular Probes) for 1 h, together with 0.25% Triton X-100 and 1% normal goat serum. Nuclei were stained with TO-PRO-3 (1:200; Molecular Probes) or DAPI (1:20000, Molecular Probes) for 5 min. Images were recorded with a confocal microscope (Olympus FluoView FV1000 and Carl Zeiss LSM700) and image analysis was carried out using ImarisColoc software (Bitmap) or Fiji (ImageJ package software) (Schindelin et al., 2012). For hNS immunocytochemical analysis, images of size 1920 × 3200 μm were acquired. Each image was divided into 84 grids of the same size and the average signal intensity was measured for each grid. The fluorescent intensity for Tuj1 was normalized to the fluorescent intensity of DAPI.

Immunohistochemical staining was performed on embryonic mice brains at E14.5 as previously described (Malmersjo et al., 2013). Three C57BL/6-129X1/SvJ *Cacna1h*$^{+/-}$ mothers ($N = 3$) were used for the immunohistochemistry staining of cortical sections. Embryos from these three mothers were genotyped to select five *Cacna1h*$^{-/-}$ and five wild-types for the analysis ($n = 10$ embryos). Briefly, brains were dissected and post-fixed in 4% PFA at 4 °C overnight. For cryoprotection, the brains were immersed in 10, 20 and 30% sucrose and frozen in OCT at −80 °C until they were used. Fourteen-micrometer frozen coronal sections were cut using a cryostat. The slides were blocked with a TSA blocking reagent (PerkinElmer, Cat. No. FP1020) for 1 h at RT and then incubated with primary antibodies for 2 h at RT. After washing, the slides were incubated for 1 h at RT with secondary antibodies. The following primary antibodies were used: rabbit-Pax6 (1:400, Covance) and mouse-MAP2 (1:400, Millipore), and following secondary antibodies: Alexa Fluor 488 anti-rabbit-IgG and Alexa Fluor 555 anti-mouse-IgG (1:400, Invitrogen). Experiments were carried out using at least one embryo from six litters for each condition. Images were recorded with a confocal microscope (Carl Zeiss LSM700) and image analysis was carried out Fiji (ImageJ package software) (Schindelin et al., 2012).

Viral transduction and cellular transfection

GIPZ Lentiviral shRNAmir against scramble RNA and *Cacna1h* was bought from Thermo Fisher Scientific Open Biosystems and co-transfected with the packaging plasmids pMD2.G and psPAX2 into HEK293T cells (Invitrogen). Virus production was performed as previously described using Lipofectamine 2000 (Invitrogen) to transfect HEK 293T cells (Tiscornia et al., 2006). The hNS cells were transduced at day 1 of differentiation and collected for further analysis on day 4. hNS cells were transfected at the same time point with Lipofectamine 2000 with control and plasmid pIRES2-EGFP containing cDNA coding for *Cacna1h*. The *Cacna1h* plasmid for overexpression analysis was a kind gift from Dr. Edward Perez-Reyes, University of Virginia School of Medicine, Charlottesville, Virginia, US.

Caspase-3 enzymatic assay

DEVD–AMC (BD biosciences) was applied to measure caspase-3 activity in hNS cells using a fluorometric assay, according to the manufacturer's protocol. The cleavage of the fluorogenic peptide substrate was monitored in a Polar Star Omega fluorometer (Bmg Labtech) using 355-nm excitation and 460-nm emission wavelengths. STS (2 μM) to trigger cell death and z-DEVD (2 μM) to inhibit caspase-3 were used as positive and negative controls, respectively.

Apoptosis assay

Differentiating hNS cells were gently dissociated at day 4 using TrypLE express (Invitrogen), collected, and stained with Annexin V-FITC conjugated antibody and Propidium Iodide (PI), following the manufacturer's protocol (BD Biosciences). Cells were analyzed with a FACSort flow cytometer (Becton Dickinson). Background fluorescence was measured using unlabeled cells and compensation was applied during analysis using single stained cells and FlowJo software (Tree Star Inc.).

Mitochondrial membrane potential analysis

Tetramethylrhodamine, ethyl ester, perchlorate (TMRE) (Molecular Probes) was added at 400 nM concentration to differentiating hNS cells 20 min before collection to detect their mitochondrial potential. One cell sample was treated with 100 nM Carbonyl cyanide 4-(trifluoromethoxy) phenylhydrazone (FCCP, Tocris) as well, which permeabilizes the inner mitochondrial membrane to protons and disrupts the membrane potential, as a negative control. Cells were then collected and resuspended in 0.2% BSA until FACS analysis. At least 10,000 cells were analyzed for each sample using a FACSort flow cytometer (Becton Dickinson). Background fluorescence was measured using unlabeled cells and compensation was applied

during analysis using single stained cells and FlowJo software (Tree Star Inc.).

Real-time PCR

Total RNA was collected from differentiating mES at days 0, 2, 4, 6, 8 and 10 and from hNS cells at day 4 using the RNeasy Mini kit (Qiagen) according to the manufacturer's instructions. RNA was quantified using NanoDrop 2000 spectrophotometer (Thermo Fisher Scientific) and SuperScript II Reverse Transcriptase (Invitrogen) and random hexamer primers (Thermo Fisher Scientific) were used for cDNA synthesis. cDNA was amplified with LightCycler 480 SYBR Green I Master Kit (Roche Life Science) and a LightCycler 1536 system (Roche Life Science). The primers used for the amplifications of both mouse and human mRNA Ca^{2+} channel families and neuronal differentiation marker genes are listed in Table 1. The PCRs were optimized to suit our conditions. PCR fragments were analyzed on agarose gel to verify product specificity. Relative gene expression was calculated using the comparative Ct method, as previously described (Pfaffl, 2001), normalized against the house keeping gene TATA-binding protein (TBP). Primers were used at a final concentration of 1 μM.

In situ hybridization

RNAscope® *in situ* hybridization (ISH) assay (Advanced Cell Diagnostics) was performed according to the manufacturer's instructions. Briefly, tissues were prepared using RNAscope Chromogenic Assay Sample Preparation for Fixed frozen tissue protocol. Embryonic (E14.5) brain slices were cut at 14 μm and hybridized with Mm-*Cacna1h* probe (ACD, Cat. No. 445461), Mm-PPIB-probe (ACD, Cat. No. 313911), and negative control probe DapB (ACD, Cat. No. 310043) at 40 °C for 2 h. ISH was performed using a 2.5 HD Assay-BROWN (ACD, Cat. No. 310035) and the images were captured using standard bright field (Inverted Microscope Olympus IX73). The image analysis was performed using Fiji (ImageJ package software) (Schindelin et al., 2012).

Subcellular fractionation assay

Mice brain cortex was dissected from E16.5 *Cacna1h* knockout mice. Protein fractionation was performed using the Subcellular Fractionation Kit (Thermo, Cat. 87790), following the manufacturer's protocol. The relative protein concentration was determined using Nanodrop 2000 (Thermo Scientific). Samples were subjected to SDS-PAGE and proteins were transferred onto nitrocellulose membranes. Western blot was performed as previously described (Zhang et al., 2009). The following antibodies were used: anti-Caspase-3 (Cell Signalling, Cat. 9662), anti-GAPDH (Sigma, Cat. G8795), and anti-HDAC2 (Sigma, Cat. SAB4300412).

Analysis of neuronal and radial glial cell distribution

Three C57BL/6-129X1/SvJ *Cacna1h*$^{+/-}$ mothers ($N = 3$) were used for the immunohistochemistry staining of cortical sections. Embryos from these three mothers were genotyped to select five *Cacna1h*$^{-/-}$ and five wild-types for the analysis ($n = 10$). Neuronal and radial glial cell distributions were analyzed using Fiji (ImageJ package software) (Schindelin et al., 2012). To define positive immunolabel signals, a relative threshold was set as the background intensity with thresholds for 488 nm (anti-Pax6), 555 nm (anti-MAP2) and 358 nm (DAPI) set at 3 times, 1.5 times, and 1 times the background intensity. Images were then binarized by defining pixels as either 1, with signals above the threshold, or zero when below their respective thresholds. To adjust

Table 1. The primers used for PCR

Gene	Forward (5′-3′)	Reverse (5′-3′)
mVDCC α1c	CGTTCTCATCCTGCTCAACA	TATGCTCCCAATGACGATGA
mVDCC α1d	TGCACAGATGAAGCCAAAAG	GACCAACGTTCTCACCGTTT
mVDCC α1g	TGTGGAAATGGTGGTGAAGA	ACTGCGGAGAAGCTGACATT
mVDCC α1h	TGGGAACGTGCTTCTTCTCT	GGGGATGTGTGAGCATTTCT
mVDCC α1a	AATTCCAAATCACGGAGCAC	CATCAGAAACGAGCACAGGA
mVDCC α1b	GCAACACATGGAACTGGTTG	GCATTCTTGTCCTCCTCTGC
mVDCC α1e	TGAAGGCTGTGTTTGACTGC	ATTCATGACGCTTCCATTCC
mPAX6	TCAGACCTCCTCATACTCGTGCA	TGTAGGTATCATAACTCCGCCCA
mhNestin	GTCAGATCGCTCAGATCCTGGA	CCAGACTAAGGGACATCTTGAGGT
mβIII Tubulin	CATGGACAGTGTTCGGTCTG	TGCAGGCAGTCACAATTCTC
mMAP2	GGTATCTGCAAGGATAGTTCAAGTAGTCAC	CCTTCTCTTGTTCTCCTTTCAGGAC
mTBP	GGGGAGCTGTGATGTGAAGT	CCAGGAAATAATTCTGGCTCA
hPAX6	TCAGACCTCCTCATACTCGTGCA	TGTAGGTATCATAACTCCGCCCA
hβIII Tubulin	CATCCAGAGCAAGAACAGCA	CTCGGTGAACTCCATCTCGT
hMAP2	AAGAAGGTCGCCATCATACG	GGCGGATGTTCTTCAGAGAG
hTBP	TATAATCCCAAGCGGTTTGC	GCTGGAAAACCCAACTTCTG
$InsP_3R1$	CCCTTCTCAGACCAGAGCAC	TGCACAATGTTGTGGGACTT
$InsP_3R2$	GGCTCGGTCAATGGCTTC	CCCCTGTTTCGCCTGCTT
$InsP_3R3$	AGAACGACCGCAGGTTTG	CCCTTGTCACGGAATGGA
RyR1	TACTTCGACACAACCCCACA	ACAGTCTCCAGCAGGGAAGA
RyR2	AGCCCTCACGACTAAAGCAA	CCACCCAGACATTAGCTGGT
RyR3	AACGTCCTGCTCTTGGAGAA	ATGTCCTCCACCTTGTCTGG

for minor differences in size in the cortical sections: (a) the row sum of the binary frequencies across the section were divided by the total number of row pixels across the section and expressed as a percentage (b) The pial surface was set as the first emergence of three consecutive percentages above zero. A stringent cutoff was set for the bottom of the ventral surface at a minimum of 50%, thus defining the normalized pial-ventral length (c) the height index was set as $(x_i/N)*100$ where N is the normalized pial-ventral length, and x_i is index number of each element from 1 to N d) to adjust for increment differences the values were summed at 5% intervals. Mean areas of fluorescent distribution were estimated according to Riemann Sums approximation of the intensity distribution curve for each cortical section.

Statistical analysis

Prior to performing the statistical tests, the Shapiro–Wilks Test was applied to assess the normality of the data distributions, and equal variance using Levene's test. Data were analyzed using either Student's unpaired *t*-test or a one-way analysis of variance (ANOVA) with Tukey's post-hoc analysis. The Bonferroni correction was applied to maintain an overall type I error rate of 0.05 against multiple comparisons. Data are presented as mean ± standard error of the mean (SEM). Sample sizes (n) represent the number of cells or brain slices and (N) represent independent repeats or animals. Statistical analyses were either conducted with SigmaPlot® 12.5 (Systat Software, Inc., San Jose, CA) or R base package (http://www.R-project.org/). Statistical significance was accepted at $^{*}P < 0.05$, $^{**}P < 0.01$, or $^{***}P < 0.001$.

RESULTS

Neural stem cells exhibit spontaneous Ca^{2+} activity

To assess the influence of Ca^{2+} signaling on neural differentiation, we analyzed mouse embryonic stem (mES) cells during neural differentiation (Fig. 1A-C) (Shi et al., 2012; Ying et al., 2003). We mapped the spontaneous Ca^{2+} activity in these cells for a period of 10 days (Fig. 2A). After 8 days of differentiation we detected a significant increase in the number of cells that exhibited spontaneous activity (8 days: 18.5 ± 7.5%, $n = 108$, $N = 4$; vs 6 days: 5.4 ± 1.2%, $n = 166$, $N = 4$; one-way ANOVA $F_{(5,16)} = 34.9$; $P = 0.005$) (Fig. 2A, C). We then tested at what day the cells became responsive to membrane depolarization by challenging them with 50 mM KCl (Fig. 2B). A clear increase in the percentage of cells showing Ca^{2+} response to this treatment occurred at day 6 (6 days: 37.1 ± 7.9%, $n = 109$, $N = 3$; vs 4 days: 2.4 ± 2.4%, $n = 147$, $N = 3$; one-way ANOVA $F_{(5,13)} = 15.04$; $P = 0.02$) (Fig. 2B, C). Both KCl-induced and spontaneous Ca^{2+} activities were dependent on external Ca^{2+} influx. Removal of extracellular Ca^{2+} from the medium abolished the KCl-induced responses (63.6 ± 10.4% vs 2.2 ± 1.5% $n = 181$, $N = 5$, $P < 0.01$) (Fig. 2D).

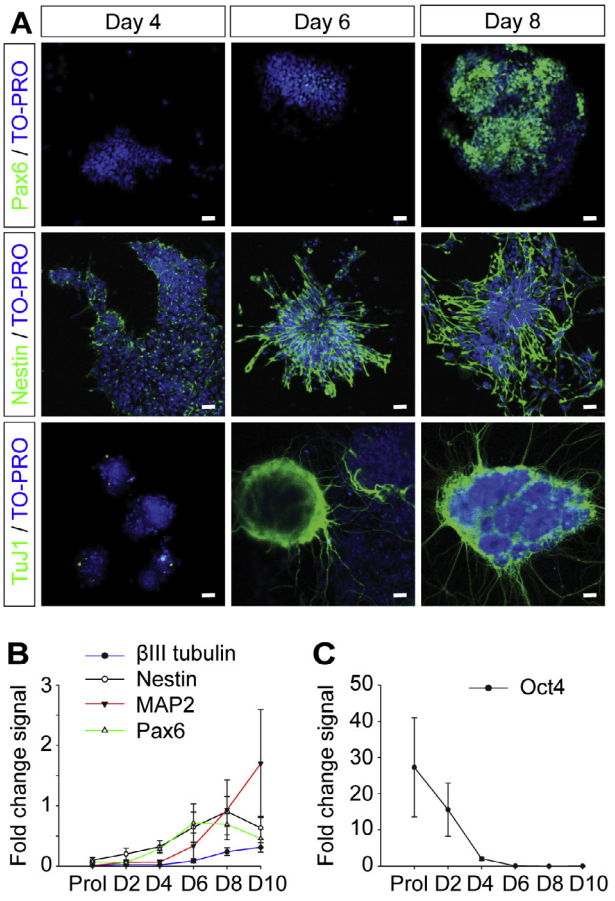

Fig. 1. Neural differentiation of mES cells. (A) Immunostaining of the neuroectodermal marker Pax6, the progenitor marker Nestin, and the neuronal marker βIII tubulin at days 4, 6 and 8 of neural differentiation of mES cells. Nuclei stained with TO-PRO. Scale bars, 10 μm. (B) mRNA expression analysis of Pax6, Nestin, βIII tubulin and MAP2 at days 0, 2, 4, 6, 8, or 10 of differentiation. (C) mRNA expression of the pluripotent stem cells marker Oct4 at days 0, 2, 4, 6, 8, or 10 of differentiation. mRNA values are expressed as $2^{-\Delta Ct}$, values are mean ± SEM.

The impact of VDCCs on the spontaneous Ca^{2+} activity in mES cells at day 8 was then tested with a pharmacological inhibitor of VDCCs. Mibefradil, a VDCC inhibitor mainly acting on T-type Ca^{2+} channels (Ertel and Ertel, 1997), used at two different concentrations, 3 μM and 30 μM, almost completely blocked the number of cells displaying spontaneous Ca^{2+} activity (3 μM: 89.3 ± 8.7% and 30 μM: 95.8 ± 2.8%; $N = 7$) (Fig. 2E). The response to membrane depolarization was partially inhibited in a number of cells by the lower concentration of Mibefradil and entirely by the high concentration (3 μM: 13.8 ± 11.3% vs 30 μM: 90.5 ± 4.7%; $N = 7$, $P < 0.005$).

We then sought out to identify genes that could be linked to the ability of cells to respond with Ca^{2+} signaling that occurred at days 6–8. We focused our attention on genes encoding essential Ca^{2+} channels, including VDCCs ($Ca_v1.2$, $Ca_v1.3$, $Ca_v2.1$, $Ca_v2.2$, $Ca_v2.3$, $Ca_v3.1$, and $Ca_v3.2$) (distinguished by the α subunit: 1 g, c, e, d, h, b, a), ryanodine receptors (RYR1-3), and inositol 1,4,5-trisphosphate receptors ($InsP_3R1$-3). Interestingly, the mRNA expression of

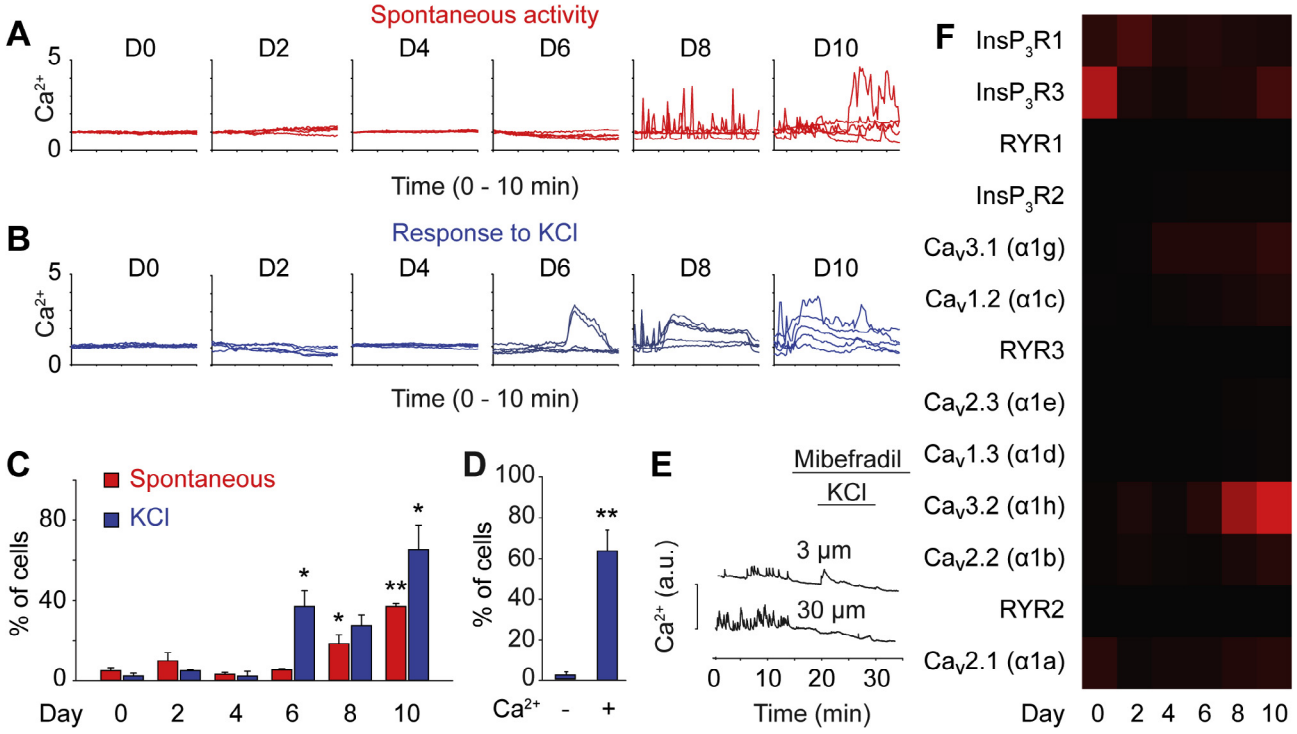

Fig. 2. Spontaneous Ca^{2+} activity is triggered by T-type Ca^{2+} channels. Representative Ca^{2+} signaling traces from mES cells exhibiting spontaneous Ca^{2+} activity (A) or challenged with 50 mM KCl (B) at days 0, 2, 4, 6, 8, or 10 of differentiation. (C) Number of cells responding with spontaneous Ca^{2+} activity (red) or to 50 mM KCl (blue) at days 0, 2, 4, 6, 8, or 10 of differentiation. (D) Number of cells responding to 50 mM KCl in Ca^{2+}-free and Ca^{2+} containing medium. (E) Two representative Ca^{2+} signaling traces from mES cells at day 8 challenged with 3 µM and 30 µM Mibefradil and then 50 mM KCl. (F) Heat map of mRNA expression levels of VDCCs, RYRs and $InsP_3Rs$ at days 0, 2, 4, 6, 8, and 10 of differentiation obtained by real-time PCR. mRNA values are expressed as $2^{-\Delta Ct}$. Values are mean ± SEM, $^{*}P < 0.05$, $^{**}P < 0.01$. (For interpretation of the references to color in this figure legend, the reader is referred to the web version of this article.)

Cacna1h that encodes the T-type Ca^{2+} channel $Ca_V3.2$ showed a dramatic increase on day 6 (Fig. 2F).

Together these results suggest that $Ca_V3.2$ is a key player for spontaneous Ca^{2+} activity in mES that undergo neural differentiation.

Spontaneous Ca^{2+} activity activates caspase-3

We continued our quest to assess the influence of Ca^{2+} signaling on neural differentiation by dividing our cells into two groups. Cells were cultured on coverslips with an etched coordinate system that enabled back-tracing after the experiment. We performed Ca^{2+} imaging and grouped cells according to their spontaneous Ca^{2+} activity (Fig. 3A). Since elevated cytosolic Ca^{2+} has been associated with increased caspase activity (Norberg et al., 2010; Orrenius et al., 2015) we assessed the association between Ca^{2+} active cells and their caspase-3 activity on a cell-to-cell basis. We observed increased cleaved caspase-3 in cells exhibiting spontaneous Ca^{2+} activity (Fig. 3B). In total 46.7 ± 3.3% of the Ca^{2+} active cells ($n = 30$, $N = 3$) showed increased caspase-3, whereas a significantly lower fraction of 20.1 ± 0.8% ($n = 30$, $N = 3$, $P < 0.005$) of the non-active cells were positive for active caspase-3 (Fig. 3C). Immunostaining for Tuj1, revealed that 41.1 ± 6.0% of the Ca^{2+} active cells ($n = 30$, $N = 3$) were positive for

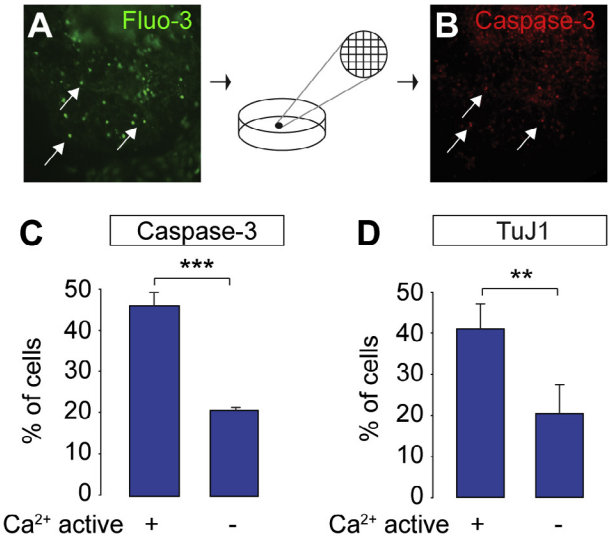

Fig. 3. Cells with spontaneous Ca^{2+} activity show activated caspase-3. (A) mES cells cultured on gridded coverslips were loaded with Fluo-3 and examined with Ca^{2+} imaging. Arrows indicate three active cells. (B) After Ca^{2+} imaging cells were immunostained for caspase-3 and analyzed according to their spontaneous Ca^{2+} activity. Arrows indicate three caspase-3 active cells. Number of cells with or without spontaneous Ca^{2+} activity stained for cleaved caspase-3 (C) or Tuj1 (D). Values are mean ± SEM, $^{**}P < 0.01$, $^{***}P < 0.001$.

Tuj1, whereas significantly fewer, 20.5 ± 7.0%, of the non-active cells (n = 30, N = 3, P < 0.05) were positive for Tuj1 (Fig. 3D). Together these data suggest that early Tuj1-positive NPCs exhibit spontaneous Ca^{2+} signaling that increases their caspase-3 activity.

Altering Cav3.2 modifies the caspase-3 activity and neural differentiation in human neuroepithelial stem cells

Next, we sought to study the interplay between $Ca_v3.2$, caspase-3, and neural differentiation in human neuroepithelial stem (hNS) cells. We first investigated if stimulating caspase-3 could modulate neural differentiation in these cells. Staurosporin (STS) is known to regulate caspase-3 activity in a dose-dependent manner (Norberg et al., 2010). Stimulating caspase-3 with a rather low dose of 100 nM STS significantly increased the fold change of βIII tubulin mRNA compared to untreated cells (1.2 ± 0.02 vs 1.0 ± 0.0, N = 3, P < 0.005) (Fig. 4A). When the cells were challenged with the caspase-3 inhibitor z-D(OMe)E(OMe)VD(OMe)-FMK (z-DEVD) the mRNA level of βIII tubulin significantly decreased (0.7 ± 0.1 vs 1.0 ± 0.0, N = 3, P < 0.05) (Fig. 4A). Procaspase activating compound-1 (PAC-1) is a small molecule zinc chelator that is specific for activating the effector pro-caspases 3/7 (Putinski et al., 2013). Differentiating hNS cells in the presence of 25 μM PAC-1 caused a significant increase in the expression of βIII tubulin, evaluated with Tuj1 immunocytochemistry, compared to controls (Ctrl: 2.0 ± 0.4 a.u., n = 252, N = 3 vs PAC-1: 2.3 ± 0.8 a.u., n = 252, N = 3; $F_{(3,1004)}$ = 25.07, P < 0.0001) (Fig. 4B). The effect of PAC-1 on βIII tubulin expression was inhibited with 20 μM z-DEVD (Ctrl: 1.98 ± 0.4 a.u., n = 252, N = 3, PAC-1 & z-DEVD: 2.1 ± 0.5 a.u., n = 252, N = 3; $F_{(3,1004)}$ = 25.07, P = 0.41) (Fig. 4B). We also analyzed if our treatments affected the number of apoptotic cells with an Annexin V assay (Fig. 4C). Only the high dose of 2 μM STS significantly increased the number of cells undergoing apoptosis (one way ANOVA $F_{(5,12)}$ = 9.679, P < 0.005) (Fig. 4C). TMRE, a positively charged dye that accumulates in active mitochondria with negatively charged membranes, was used to study the possible involvement of the mitochondria. The number of cells that incorporated TMRE significantly increased when cells were pre-treated with Mibefradil (1.4 ± 0.05 a.u., N = 2, vs 1.0 ± 0.0 a.u., N = 2, $F_{(3,4)}$ = 102.8, P < 0.05) and z-DEVD (1.3 ± 0.07 a.u., N = 2, vs 1.0 ± 0.0 a.u., N = 2, $F_{(3,4)}$ = 102.8, P = 0.067) (Fig. 4D), while pre-treatment with 2 μM STS significantly reduced the number of cells stained by TMRE (0.3 ± 0.04 a.u., N = 2, vs 1.0 ± 0.0 a.u., N = 2, $F_{(3,4)}$ = 102.8, P < 0.005) (Fig. 4D).

Next, we examined the subcellular expression pattern of caspase-3, as it was previously shown that nuclear caspase-3 is a pro-apoptotic marker (Kamada et al., 2005). No significant nuclear expression of caspase-3 was observed when cells were treated with either Mibefradil, KCl, or 100 nM STS (Fig. 4E, F). The higher dose of 2 μM STS, however, significantly increased the amount of nuclear caspase-3 in hNS cells (STS 2 μM: 2.0 ± 0.08 vs Ctrl: 1.0 ± 0.2, one-way ANOVA $F_{(5,30)}$ = 66.46; P < 0.00001) (Fig. 4E, F). When inhibiting caspase-3 with z-DEVD, a significant reduction in nuclear staining was detected (z-DEVD: 0.7 ± 0.1 vs Ctrl: 1.0 ± 0.2, one-way ANOVA $F_{(5,30)}$ = 66.46; P = 0.007) (Fig. 4E, F).

To investigate the specific role of $Ca_v3.2$ later during neural differentiation we altered its mRNA expression levels by targeting the *CACNA1H* gene with viral infections. Knocking down *CACNA1H* mRNA expression by 49 ± 19% gave significantly decreased DEVDase activity (1.0 ± 0.0 a.u. vs 0.9 ± 0.02 a.u., n = 3, P < 0.05) (Fig. 4G). When *CACNA1H* mRNA was overexpressed we observed a slight but non-significant increase in DEVDase activity (1.0 ± 0.0 a.u. vs 1.04 ± 0.05 a.u., n = 3, P = 0.55) (Fig. 4G). We next assessed the impact of altering the mRNA levels of *CACNA1H* on expression markers Pax6, Nestin, βIII tubulin, and MAP2. Knockdown of *CACNA1H* had sparse effects on the mRNA expressions of the early neuronal markers Pax6 (1.0 ± 0.1 a.u., n = 3, N = 3, P = 0.88), Nestin (1.1 ± 0.04 a.u., n = 3, N = 3, P = 0.08) and MAP2 (0.9 ± 0.1 a.u., n = 3, N = 3, P = 0.39) (Fig. 4H, I, K), whereas βIII tubulin mRNA significantly decreased compared to controls in *CACNA1H* siRNA lentiviral vector-transduced cells (0.8 ± 0.03 a.u., n = 3, N = 3, P < 0.05) (Fig. 4J). We thereafter overexpressed *CACNA1H* and detected a significant Pax6 decrease (0.9 ± 0.02 a.u., n = 3, N = 3, P < 0.001) and βIII tubulin increased (1.2 ± 0.06 a.u., n = 3, N = 3, P < 0.05) in lentiviral vector-transduced cells (Fig. 4H, J). Overexpression had little effect on the transition from the proliferative state (seen with Pax6) to early immature post mitotic cells before the onset of more mature NPC states occupying the CP (seen with MAP2). Namely, taken together these data indicate that altering *CACNA1H* affects both caspase-signaling and neural differentiation without affecting apoptosis.

Cacna1h in the embryonic mice

Next, we sought to investigate *Cacna1h* gene expression and function in the mouse brain. We characterized the expression of *Cacna1h* mRNA *in vivo* using RNAscope *in situ* hybridization. The *Cacna1h* probe was detected in the cortex region (Fig. 5A) including the CP (Fig. 5B) and SVZ/VZ (Fig. 5C) of C57BL/6 mice at E14.5. Similar expression patterns of the *Cacna1h* probe were observed in 129*1/SVJ mice (data not shown). We then performed Ca^{2+} recordings in slices from C57BL/6 mice with 2-photon laser scanning microscopy. These experiments showed that differentiating NPCs in the embryonic mouse cortex were exhibiting spontaneous Ca^{2+} activity at E16.5 (Fig. 5D, F). To investigate the specific role of $Ca_v3.2$ we then monitored Ca^{2+} signaling in *Cacna1h* knockout mice. We observed that the spontaneous Ca^{2+} activity in the cortical region of knockout mice was significantly decreased (WT: 25.6 ± 3.9%, n = 603, N = 3; vs KO: 12.6 ± 1.6%, n = 375, N = 3; P < 0.05) (Fig. 5F). We thereafter examined if the caspase-3 expression pattern differed between wild-type and knockout animals. We performed

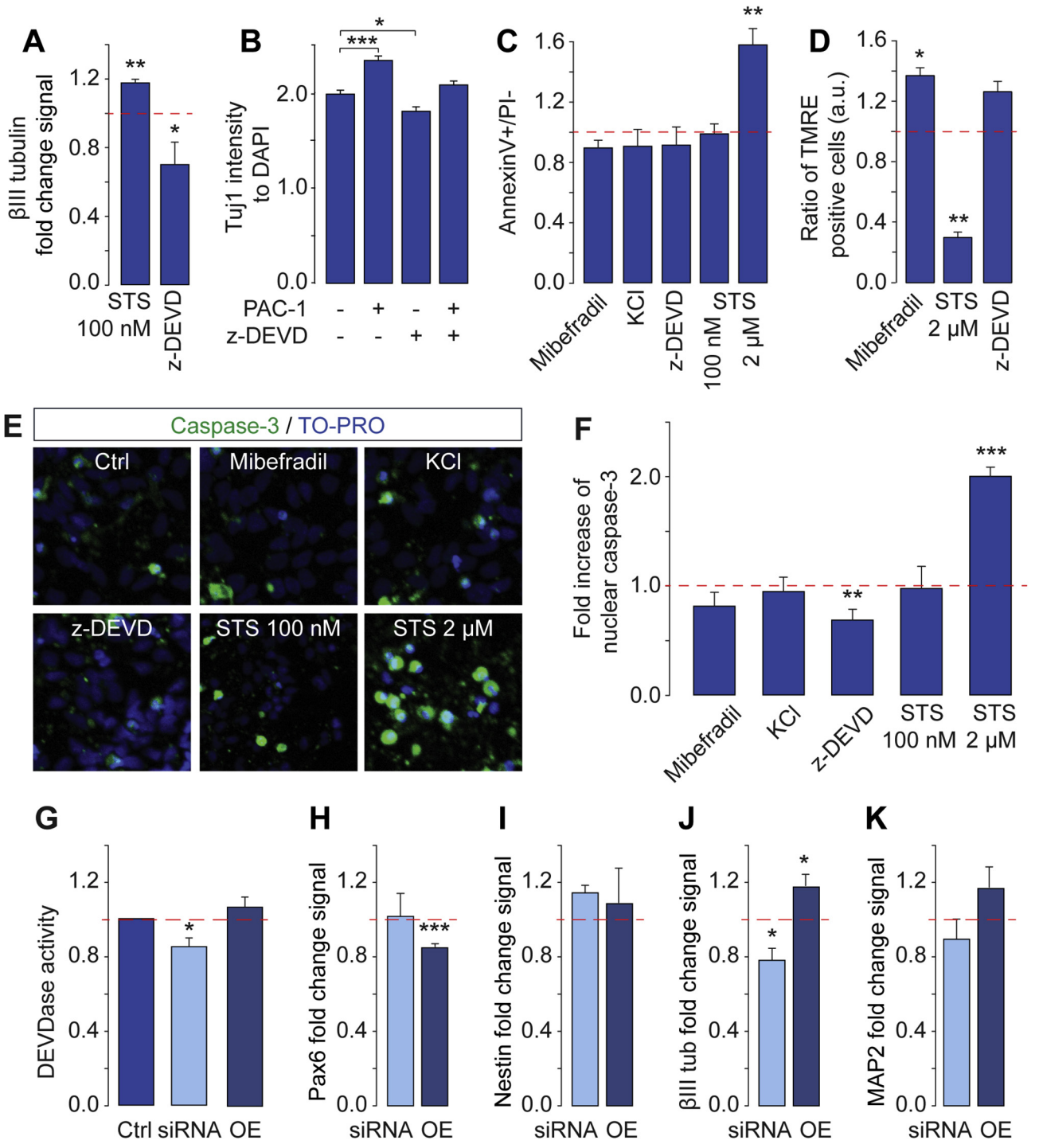

Fig. 4. $Ca_v3.2$ activates caspase-3 and regulates neural differentiation. (A) mRNA expression level of βIII tubulin in hES cells at day 4 of differentiation treated with 100 nM STS or 2 μM z-DEVD. (B) Tuj1 fluorescent intensity normalized to DAPI of hES cells at day 4 of differentiation treated with 25 μM PAC-1, 20 μM z-DEVD, or both PAC-1 and z-DEVD. (C) Annexin V + /PI − staining of hES cells at day 4 of differentiation treated with 3 μM Mibefradil, 12 mM KCl, 2 μM z-DEVD, 100 nM STS or 2 μM STS. (D) Ratio of TMRE-positive cells to respective controls (arbitrary units a. u.) of cells pretreated with 3 μM Mibefradil, 2 μM STS or 2 μM z-DEVD. (E) Caspase-3 immunostaining of hES cells at day 4 of differentiation treated with 3 μM Mibefradil, 12 mM KCl, 2 μM z-DEVD, 100 nM STS or 2 μM STS. Nuclei stained with TO-PRO. (F) Quantification of nuclear caspase-3 with indicated treatments. (G) DEVDase activity in hES cells at day 4 of differentiation with siRNA knock-down or overexpression of *CACNA1H*. (H-K) mRNA expression level of Pax6, Nestin, βIII tubulin and MAP2 in hES cells at day 4 of differentiation with siRNA knock-down or overexpression of *CACNA1H*. mRNA values are expressed as $2^{-\Delta\Delta Ct}$. For H-K, unpaired Student's *t*-test was conducted between each treatment and its respective control. Values are mean ± SEM, $^{*}P < 0.05$, $^{**}P < 0.01$, $^{***}P < 0.001$.

Western blot analyses of cytosolic and nuclear fractions from the cortex region of E16.5 mice (Fig. 5G). Cleaved caspase-3 was detected only in cytosolic fractions. Interestingly, cleaved caspase-3 expression level was significantly lower in knockout mice in comparison to wild-type controls (19-kDa Caspase-3: WT 1.3 ± 0.3 a.

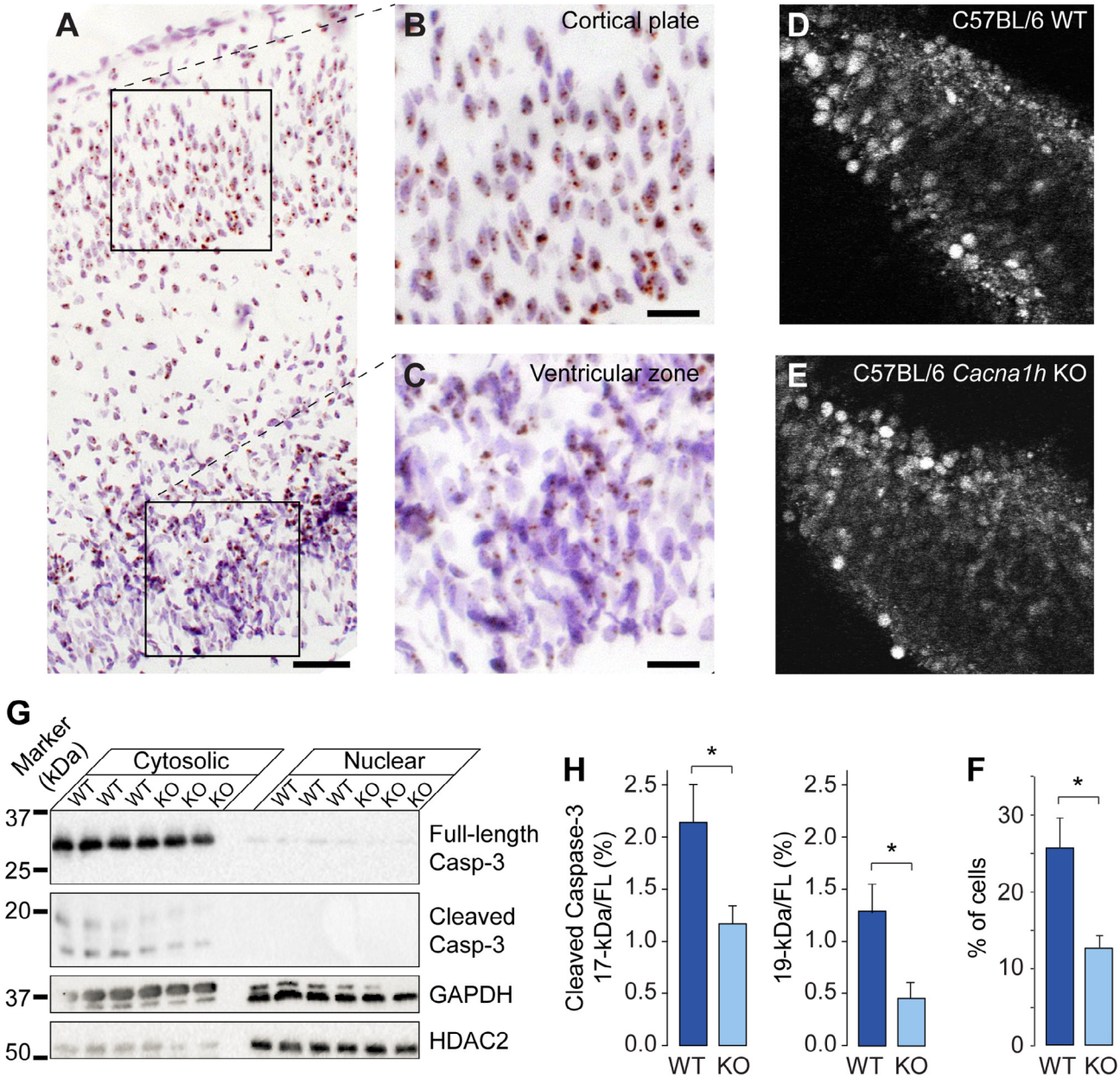

Fig. 5. *Cacna1h* RNA is expressed in the cortical region of embryonic brain and regulates spontaneous Ca^{2+} activity. RNAscope *in situ* hybridization of embryonic brain slices at E14.5 from C57BL/6 mouse (A), CP (B), and VZ (C). Cells were stained with hematoxylin 50% (purple), *Cacna1h* mRNA were stained with DAB (brown). Scale bars 50 μm (A) and 20 μm (B, C). 2-photon microscopy images of Fluo-4/AM loaded coronal slices from C57BL/6 WT (D) and *Cacna1h* knockout (KO, E) E16.5 animals. (F) Number of cells with spontaneous Ca^{2+} activity in slices from C57BL/6 WT and *Cacna1h* knockout E16.5 animals. (G) Western blot analysis of full-length and cleaved caspase-3 in brains from C57BL/6 WT and *Cacna1h* knockout E16.5 animals. Cytosolic and nuclear cleaved caspase-3 (17-kDA and 19-kDa), GAPDH (37-kDa) and HDAC2 (55-kDa) proteins were detected. (H) Cytosolic cleaved caspase-3 (*left panel:* 17-kDa and *right panel* 19-kDa) values were calculated as the ratio of cleaved caspase-3 to full-length caspase-3 (FL). Values are mean ± SEM, $^{*}P < 0.05$, $^{**}P < 0.01$, $^{***}P < 0.001$. (For interpretation of the references to color in this figure legend, the reader is referred to the web version of this article.)

u. vs KO 0.5 ± 0.1 a.u., $N = 3$, $P < 0.05$; 17-kDa Caspase-3: WT 2.1 ± 0.4 a.u. vs KO 1.2 ± 0.2 a.u., $N = 3$; $P < 0.05$) (Fig. 5H).

Cacna1h knockout reduces the size of SVZ/VZ and CP zones in 129X1/SvJ mice

Finally, we tested the influence of $Ca_v3.2$ on neocortical development in the brains of *Cacna1h* knockout mice. We carried out experiments on C57BL/6 *Cacna1h* knockout crossed with 129X1/SvJ (SvJ/BL6) and compared for possible cortical abnormalities between wild-type and *Cacna1h* knockout (Fig. 6A, B). We stained for Pax6 and MAP2, which are markers of cells residing in the VZ/SVZ or CP regions, respectively. Interestingly, we observed significant decreases in the density of radial glial cells in the VZ and neurons in the CP in *Cacna1h* knockout SvJ/BL6 (E14.5) animals (Fig. 6C). We observed a modest but significant reduction in the size of the CP (1.0 ± 0.07 vs 0.7

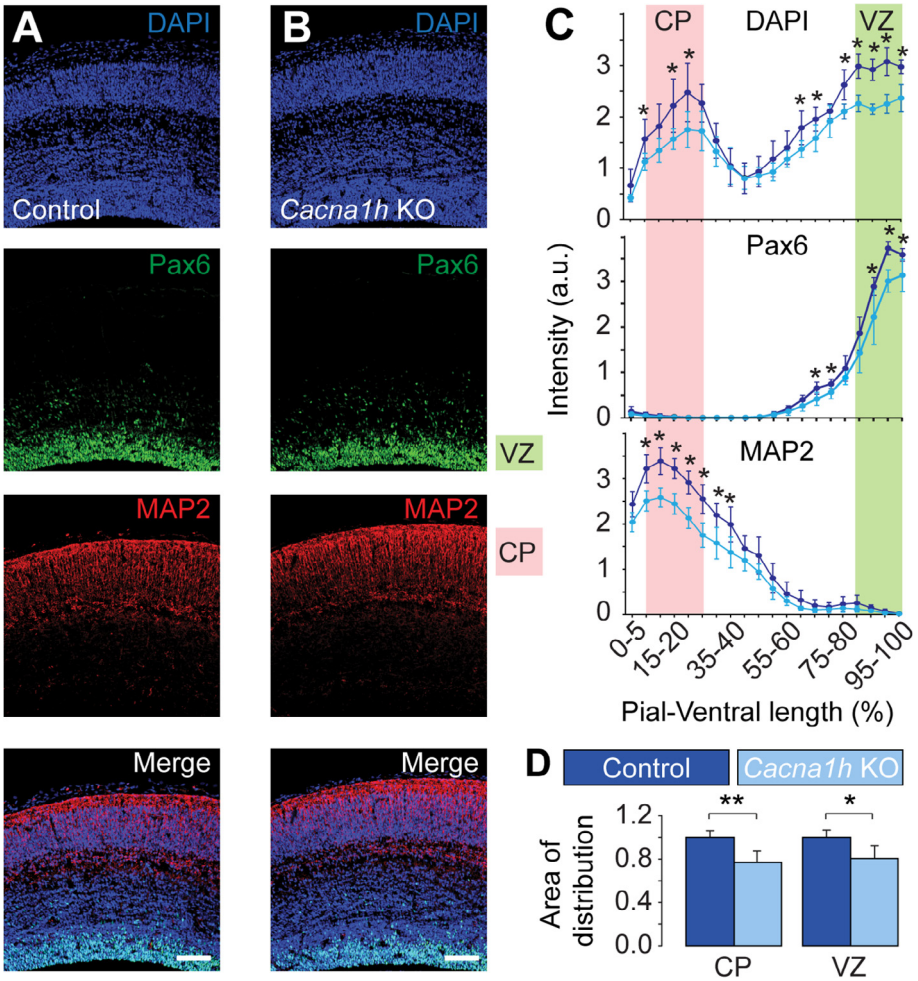

Fig. 6. The VZ is smaller in *Cacna1h* knockout brains. Immunohistochemistry staining of Pax6 and MAP2 in E14.5 brain slices from SvJ/BL6 control (A) and *Cacna1h* knockout (KO) (B). Nuclei stained with DAPI. (C) Density plots of the fluorescence signal of DAPI, Pax6, and MAP2 in the cortical region in SvJ/BL6 control and *Cacna1h* knockout mice. Unpaired Student's *t*-test was conducted between each KO region and its respective WT control region (D) Statistical analysis of the sizes of the VZ and CP of E14.5 brain slices from SvJ/BL6 WT ($n = 5$, $N = 3$) and *Cacna1h* knockout animals ($n = 5$, $N = 3$). Scale bars 100 μm. Values are mean ± SEM, $^{*}P < 0.05$, $^{**}P < 0.01$.

± 0.01 a.u., $n = 5$, $N = 3$, $P < 0.005$) and SVZ/VZ (1.0 ± 0.07 vs 0.8 ± 0.1 a.u., $n = 5$, $N = 3$, $P < 0.05$) in *Cacna1h* knockout animals (Fig. 6D). Together these data show that $Ca_v3.2$ is a critical player of embryonic brain development.

DISCUSSIONS

It is well known that $Ca_v3.2$ channels play a significant role in a large number of physiological and pathological processes in adults (Cheong and Shin, 2013; Hortenhuber et al., 2017; Panner and Wurster, 2006). However, less is known about their roles in the developing brain. Interestingly, T-type Ca^{2+} channels are highly expressed very early during neuronal development, even before the onset of L-, N-, P/Q- and R-type Ca^{2+} channels (Chemin et al., 2002; Ohkubo and Yamazaki, 2012; Yanagida et al., 2004) (www.emouseatlas.org, www.brain-map.org). Here we show that $Ca_v3.2$ plays a critical role in modulating neural differentiation during brain development.

Spontaneous Ca^{2+} waves have been reported in the developing central nervous system (Spitzer, 2006; Weissman et al., 2004) and in stem cells (Ciccolini et al., 2003; Malmersjo et al., 2013). We observed that the origin of spontaneous Ca^{2+} activity correlated in time with the rise in expression of $Ca_v3.2$ mRNA suggesting its involvement in driving this signaling event. This assumption was verified by the fact that the spontaneous Ca^{2+} activity was abolished when cells were treated with an inhibitor of $Ca_v3.2$. The impact of T-type channels on spontaneous Ca^{2+} activity has not only been reported previously in neural cells (Barone et al., 2004), but also in cardiac cells (Chiang et al., 2009) and breast cancer cells (Ohkubo and Yamazaki, 2012). These and other reports show that T-type channels have diverse roles both in health and disease. We speculate that regulation of *CACNA1H* expression levels serves as a molecular switch that critically regulates spontaneous Ca^{2+} activity in individual cells and subsequently provides a bifurcation point for the underlying gene regulatory networks involved in cell fate determination.

A number of reports have described a crucial role for caspase-3 in regulating differentiation (Abdul-Ghani and Megeney, 2008; Bell and Megeney, 2017; Bulatovic et al., 2015; D'Amelio et al., 2012; Unsain and Barker, 2015). The results presented herein demonstrate a novel interaction between $Ca_v3.2$ channel activity and caspase-3 during neurogenesis. The responsible downstream target(s) of caspase-3 in regulating differentiation remain unknown. Our results with the mitochondrial membrane potential dye suggest an involvement of the mitochondria during *Cacna1h* and caspase-3 activity (seen with the effect of Mibefradil and z-DEVD). It would be tempting to hypothesize that the intrinsic pathway, under constitutive modulation by T-type Ca^{2+} channels, is involved in activating sublethal concentrations of caspase-3 via quantal release of cytochrome-c and caspase-9 activation (Unsain and Barker, 2015). Nonetheless, further work will be needed to thoroughly address this question. Additionally, an increase in cytosolic Ca^{2+} can activate both caspases and calpains (Chan and Mattson, 1999), which regulate

the processes of differentiation, apoptosis and necrosis. A fine regulation of caspases versus calpains may be the determining factor that decides cell fate.

Experiments on $Ca_v3.2$-knockout mice showed an attenuation of spontaneous Ca^{2+} activity in the brain of these animals and a significant reduction in the level of cleaved caspase-3 proteins. Furthermore, small but significant differences were detected in the size of the VZ/SVZ and CP between knockout and wild-type animals. Interestingly, we only observed this difference in 129X1/SvJ animals, which are reported to have caspase sensitivity (Leonard et al., 2002). This knockout is not lethal for the mouse and they have been reported to have abnormal blood vessel morphology, cardiac fibrosis, and deficiencies in context-associated memory, other than reduced size (Chen et al., 2003b; Chen et al., 2012). The fact that this knockout is not lethal may suggest that it could play a role for other cognitive dysfunctions, e.g., epilepsy or autism. Behavioral studies on 8–12-week-old mice with *Cacna1h* gene deletion have been reported to induce anxiety-like phenotypes, impairment of hippocampus-dependent recognition memories and reduced sensitivity to psychostimulants (Gangarossa et al., 2014). Furthermore, human *CACNA1H* gene mutations have been associated with autism spectrum disorder (Splawski et al., 2006). Such disorders were suggested to have a possible neurodevelopmental etiology (Parellada et al., 2014).

In summary, we report a novel signaling mechanism that connects Ca^{2+} entry through $Ca_v3.2$ with caspase-3 activation that regulates the differentiative capacity of NPCs during corticogenesis.

ACKNOWLEDGMENTS

This work was supported by the Swedish Brain Foundation (grant FO2017-0107 and FO2018-0209 to PU), the Swedish Research Council (2013-3189 and 2017-00815 to PU), the Swedish Cancer Society (grant CAN 2013-802 and CAN 2016-801 to PU), Linnaeus Center in Developmental Biology for Regenerative Medicine, the Karolinska Institute's KID doctoral program (to PR and DK), Åke Wiberg's Foundation (to PU), Magnus Bergvall's Foundation (to PU), Fredrik and Ingrid Thuring's Foundation (to PU), and the Swedish Society for Medical Research (to PU), the Wenner-Gren Foundation (to SK), and Japan Society for the Promotion of Science (to SK), the Scandinavia-Japan Sasakawa Foundation (to SK), and The Sigrid Jusélius Foundation (to LL).

Competing interests

The authors declare no competing financial interests.

REFERENCES

Abdul-Ghani M, Megeney LA (2008) Rehabilitation of a contract killer: caspase-3 directs stem cell differentiation. Cell Stem Cell 2:515–516.

Barone F, Aguanno S, D'Alessio A, D'Agostino A (2004) Sertoli cell modulates MAA-induced apoptosis of germ cells throughout voltage-operated calcium channels. FASEB J 18:353–354.

Bell RAV, Megeney LA (2017) Evolution of caspase-mediated cell death and differentiation: twins separated at birth. Cell Death Differ 24:1359–1368.

Bulatovic I, Ibarra C, Osterholm C, Wang H, Beltran-Rodriguez A, Varas-Godoy M, Mansson-Broberg A, Uhlen P, et al. (2015) Sublethal caspase activation promotes generation of cardiomyocytes from embryonic stem cells. Plos One 10 e0120176.

Cano-Abad MF, Villarroya M, Garcia AG, Gabilan NH, Lopez MG (2001) Calcium entry through L-type calcium channels causes mitochondrial disruption and chromaffin cell death. J Biol Chem 276:39695–39704.

Catterall WA (2011) Voltage-gated calcium channels. Csh Perspect Biol 3.

Chan SL, Mattson MP (1999) Caspase and calpain substrates: roles in synaptic plasticity and cell death. J Neurosci Res 58:167–190.

Chemin J, Nargeot J, Lory P (2002) Neuronal T-type alpha 1H calcium channels induce neuritogenesis and expression of high-voltage-activated calcium channels in the NG108-15 cell line. J Neurosci 22:6856–6862.

Chen CC, Lamping KG, Nuno DW, Barresi R, Prouty SJ, Lavoie JL, Cribbs LL, England SK, et al. (2003a) Abnormal coronary function in mice deficient in alpha1H T-type Ca2+ channels. Science 302:1416–1418.

Chen CC, Shen JW, Chung NC, Min MY, Cheng SJ, Liu IY (2012) Retrieval of context-associated memory is dependent on the Ca (v)3.2 T-type calcium channel. Plos One 7.

Chen YC, Lu JJ, Pan H, Zhang YH, Wu HS, Xu KM, Liu XY, Jiang YW, et al. (2003b) Association between genetic variation of CACNA1H and childhood absence epilepsy. Ann Neurol 54:239–243.

Cheng YC, Huang CJ, Lee YJ, Tien LT, Ku WC, Chien R, Lee FK, Chien CC (2016) Knocking down of heat-shock protein 27 directs differentiation of functional glutamatergic neurons from placenta-derived multipotent cells. Sci Rep 6:30314.

Cheong E, Shin HS (2013) T-type Ca2+ channels in normal and abnormal brain functions. Physiol Rev 93:961–992.

Chiang CS, Huang CH, Chieng H, Chang YT, Chang D, Chen JJ, Chen YC, Chen YH, et al. (2009) The Ca(v)3.2 T-type Ca(2+) channel is required for pressure overload-induced cardiac hypertrophy in mice. Circ Res 104:522–530.

Ciccolini F, Collins TJ, Sudhoelter J, Lipp P, Berridge MJ, Bootman MD (2003) Local and global spontaneous calcium events regulate neurite outgrowth and onset of GABAergic phenotype during neural precursor differentiation. J Neurosci 23:103–111.

D'Amelio M, Sheng M, Cecconi F (2012) Caspase-3 in the central nervous system: beyond apoptosis. Trends Neurosci 35:700–709.

Ertel SI, Ertel EA (1997) Low-voltage-activated T-type Ca2+ channels. Trends Pharmacol Sci 18:37–42.

Falk A, Koch P, Kesavan J, Takashima Y, Ladewig J, Alexander M, Wiskow O, Tailor J, et al. (2012) Capture of neuroepithelial-like stem cells from pluripotent stem cells provides a versatile system for in vitro production of human neurons. Plos One 7 e29597.

Fan W, Dai Y, Xu H, Zhu X, Cai P, Wang L, Sun C, Hu C, et al. (2013) Caspase-3 modulates regenerative response after stroke. Stem Cells.

Fernando P, Brunette S, Megeney LA (2005) Neural stem cell differentiation is dependent upon endogenous caspase 3 activity. FASEB J 19:1671–1673.

Gangarossa G, Laffray S, Bourinet E, Valjent E (2014) T-type calcium channel Cav3.2 deficient mice show elevated anxiety, impaired memory and reduced sensitivity to psychostimulants. Front Behav Neurosci 8:92.

Gaspard N, Bouschet T, Hourez R, Dimidschstein J, Naeije G, van den Ameele J, Espuny-Camacho I, Herpoel A, et al. (2008) An intrinsic mechanism of corticogenesis from embryonic stem cells. Nature 455:351–357.

Giorgi C, Danese A, Missiroli S, Patergnani S, Pinton P (2018) Calcium dynamics as a machine for decoding signals. Trends Cell Biol 28:258–273.
Heron SE, Khosravani H, Varela D, Bladen C, Williams TC, Newman MR, Scheffer IE, Berkovic SF, et al. (2007) Extended spectrum of idiopathic generalized epilepsies associated with CACNA1H functional variants. Ann Neurol 62:560–568.
Hortenhuber M, Toledo EM, Smedler E, Arenas E, Malmersjo S, Louhivuori L, Uhlen P (2017) Mapping genes for calcium signaling and their associated human genetic disorders. Bioinformatics 33:2547–2554.
Kamada S, Kikkawa U, Tsujimoto Y, Hunter T (2005) Nuclear translocation of caspase-3 is dependent on its proteolytic activation and recognition of a substrate-like protein(s). J Biol Chem 280:857–860.
Kriegstein AR, Gotz M (2003) Radial glia diversity: a matter of cell fate. Glia 43:37–43.
Lanneau D, de Thonel A, Maurel S, Didelot C, Garrido C (2007) Apoptosis versus cell differentiation: role of heat shock proteins HSP90, HSP70 and HSP27. Prion 1:53–60.
Leonard JR, Klocke BJ, D'Sa C, Flavell RA, Roth KA (2002) Strain-dependent neurodevelopmental abnormalities in caspase-3-deficient mice. J Neuropathol Exp Neurol 61:673–677.
Li Z, Jo J, Jia JM, Lo SC, Whitcomb DJ, Jiao S, Cho K, Sheng M (2010) Caspase-3 activation via mitochondria is required for long-term depression and AMPA receptor internalization. Cell 141:859–871.
Lory P, Bidaud I, Chemin J (2006) T-type calcium channels in differentiation and proliferation. Cell Calcium 40:135–146.
Louhivuori LM, Louhivuori V, Wigren HK, Hakala E, Jansson LC, Nordstrom T, Castren ML, Akerman KE (2013) Role of low voltage activated calcium channels in neuritogenesis and active migration of embryonic neural progenitor cells. Stem Cells Dev 22:1206–1219.
Malmersjo S, Rebellato P, Smedler E, Planert H, Kanatani S, Liste I, Nanou E, Sunner H, et al. (2013) Neural progenitors organize in small-world networks to promote cell proliferation. Proc Natl Acad Sci U S A 110:E1524–E1532.
Merendino L, Guth S, Bilbao D, Martinez C, Valcarcel J (1999) Inhibition of msl-2 splicing by Sex-lethal reveals interaction between U2AF35 and the 3' splice site AG. Nature 402:838–841.
Mukasa T, Urase K, Momoi MY, Kimura I, Momoi T (1997) Specific expression of CPP32 in sensory neurons of mouse embryos and activation of CPP32 in the apoptosis induced by a withdrawal of NGF. Biochem Biophys Res Commun 231:770–774.
Norberg E, Karlsson M, Korenovska O, Szydlowski S, Silberberg G, Uhlen P, Orrenius S, Zhivotovsky B (2010) Critical role for hyperpolarization-activated cyclic nucleotide-gated channel 2 in the AIF-mediated apoptosis. EMBO J 29:3869–3878.
Ohkubo T, Yamazaki J (2012) T-type voltage-activated calcium channel Cav3.1, but not Cav3.2, is involved in the inhibition of proliferation and apoptosis in MCF-7 human breast cancer cells. Int J Oncol 41:267–275.
Orrenius S, Gogvadze V, Zhivotovsky B (2015) Calcium and mitochondria in the regulation of cell death. Biochem Biophys Res Commun 460:72–81.
Panner A, Wurster RD (2006) T-type calcium channels and tumor proliferation. Cell Calcium 40:253–259.
Parellada M, Penzol MJ, Pina L, Moreno C, Gonzalez-Vioque E, Zalsman G, Arango C (2014) The neurobiology of autism spectrum disorders. Eur Psychiatry 29:11–19.
Perez-Reyes E, Lory P (2006) Molecular biology of T-type calcium channels. Cns Neurol Disord-Dr 5:605–609.
Pfaffl MW (2001) A new mathematical model for relative quantification in real-time RT-PCR. Nucleic Acids Res 29 e45.
Pompeiano M, Blaschke AJ, Flavell RA, Srinivasan A, Chun J (2000) Decreased apoptosis in proliferative and postmitotic regions of the Caspase 3-deficient embryonic central nervous system. J Comp Neurol 423:1–12.
Putinski C, Abdul-Ghani M, Stiles R, Brunette S, Dick SA, Fernando P, Megeney LA (2013) Intrinsic-mediated caspase activation is essential for cardiomyocyte hypertrophy. Proc Natl Acad Sci U S A 110:E4079–E4087.
Rodriguez-Gomez JA, Levitsky KL, Lopez-Barneo J (2012) T-type Ca2+ channels in mouse embryonic stem cells: modulation during cell cycle and contribution to self-renewal. Am J Physiol Cell Physiol 302:C494–C504.
Rohn TT, Cusack SM, Kessinger SR, Oxford JT (2004) Caspase activation independent of cell death is required for proper cell dispersal and correct morphology in PC12 cells. Exp Cell Res 295:215–225.
Schindelin J, Arganda-Carreras I, Frise E, Kaynig V, Longair M, Pietzsch T, Preibisch S, Rueden C, et al. (2012) Fiji: an open-source platform for biological-image analysis. Nat Methods 9:676–682.
Senatore A, Spafford JD (2012) Gene transcription and splicing of T-type channels are evolutionarily-conserved strategies for regulating channel expression and gating. Plos One 7.
Shi Y, Kirwan P, Smith J, Robinson HP, Livesey FJ (2012) Human cerebral cortex development from pluripotent stem cells to functional excitatory synapses. Nat Neurosci 15(477–486):S471.
Shin HS, Cheong EJ, Choi S, Lee J, Na HS (2008) T-type Ca2+ channels as therapeutic targets in the nervous system. Curr Opin Pharmacol 8:33–41.
Smedler E, Uhlen P (2014) Frequency decoding of calcium oscillations. Bba-Gen Subjects 1840:964–969.
Spitzer NC (2006) Electrical activity in early neuronal development. Nature 444:707–712.
Splawski I, Yoo DS, Stotz SC, Cherry A, Clapham DE, Keating MT (2006) CACNA1H mutations in autism spectrum disorders. J Biol Chem 281:22085–22091.
Tiscornia G, Singer O, Verma IM (2006) Production and purification of lentiviral vectors. Nat Protoc 1:241–245.
Uhlen P, Fritz N (2010) Biochemistry of calcium oscillations. Biochem Bioph Res Co 396:28–32.
Uhlen P, Fritz N, Smedler E, Malmersjo S, Kanatani S (2015) Calcium signaling in neocortical development. Dev Neurobiol 75:360–368.
Unsain N, Barker PA (2015) New views on the misconstrued: executioner caspases and their diverse non-apoptotic roles. Neuron 88:461–474.
Wang R, Lewin GR (2011) The Ca(v)3.2 T-type calcium channel regulates temporal coding in mouse mechanoreceptors. J Physiol-London 589:2229–2243.
Weissman TA, Riquelme PA, Ivic L, Flint AC, Kriegstein AR (2004) Calcium waves propagate through radial glial cells and modulate proliferation in the developing neocortex. Neuron 43:647–661.
Yan XX, Najbauer J, Woo CC, Dashtipour K, Ribak CE, Leon M (2001) Expression of active caspase-3 in mitotic and postmitotic cells of the rat forebrain. J Comp Neurol 433:4–22.
Yanagida E, Shoji S, Hirayama Y, Yoshikawa F, Otsu K, Uematsu H, Hiraoka M, Furuichi T, et al. (2004) Functional expression of Ca2+ signaling pathways in mouse embryonic stem cells. Cell Calcium 36:135–146.
Ying QL, Stavridis M, Griffiths D, Li M, Smith A (2003) Conversion of embryonic stem cells into neuroectodermal precursors in adherent monoculture. Nat Biotechnol 21:183–186.
Zhang S, Hisatsune C, Matsu-Ura T, Mikoshiba K (2009) G-protein-coupled receptor kinase-interacting proteins inhibit apoptosis by inositol 1,4,5-triphosphate receptor-mediated Ca2+ signal regulation. J Biol Chem 284:29158–29169.
Zhong XL, Liu JRR, Kyle JW, Hanck DA, Agnew WS (2006) A profile of alternative RNA splicing and transcript variation of CACNA1H, a human T-channel gene candidate for idiopathic generalized epilepsies. Hum Mol Genet 15:1497–1512.

(Received 5 July 2018, Accepted 12 January 2019)
(Available online 21 January 2019)